Electronic Supplementary Information for

Ce stabilized Ni-SrO as a catalytic phase transition sorbent for integrated CO_2 capture and CH_4 reforming

Haiming Gu [a,b] , Yunfei Gao [a,c,*], Sherafghan Iftikhar [a], Fanxing Li [a,*]

a, Department of Chemical and Biomolecular Engineering, North Carolina State University, Raleigh, NC 27695-7905, United States

b, School of Energy and Power Engineering, Nanjing Institute of Technology, Nanjing 211167, China

c, Key Laboratory of Coal Gasification and Energy Chemical Engineering of Ministry of Education, Shanghai Engineering Research Center of Coal Gasification, East China University of Science and Technology, Shanghai 200237, China

This Supplementary information contains the following Figures:

* Author to whom correspondence should be addressed

E-mail address: ygao9@ncsu.edu (Y. Gao), fli5@ncsu.edu (F. Li).

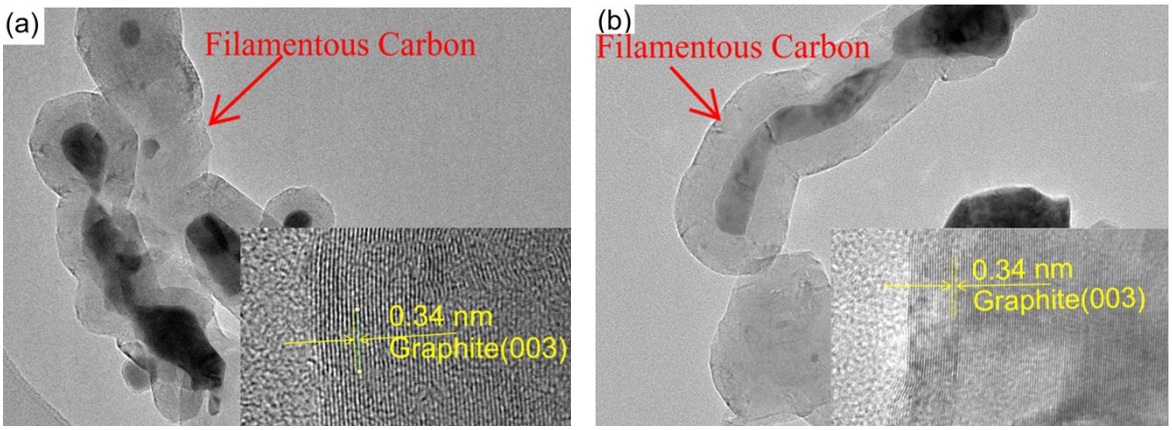

Figure S1: HRTEM images of sorbents: (a) reacted $SrCe_{0.5}Ni_{0.5}$ and (b) reacted SrNi.

The reactivity of catalyst is vital to CH_4 conversion, and the carbon deposition during this SLDRM process would block the catalyst active site causing reactivity deterioration. The carbon deposition could be mainly classified into amorphous and nanotube carbon with different property. Figure S1 shows the HRTEM analysis for $SrCe_{0.5}Ni_{0.5}$ and SrNi to evaluate type of carbon deposition. The HRTEM images (Figures S1(a) and S1(b)) indicate that filamentous carbon formed on both materials, and the lattice space corresponded to graphite.

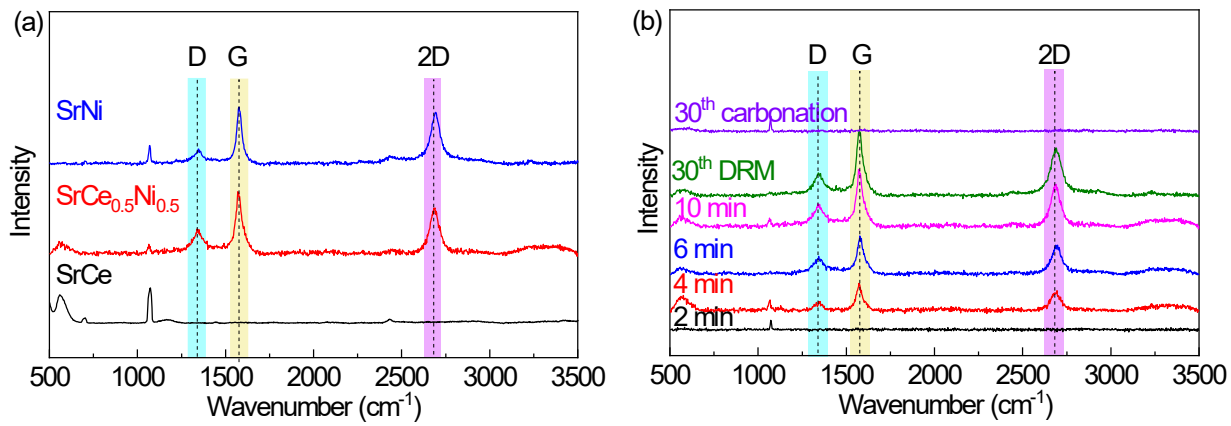

Figure S2: Raman analysis carbon deposition on (a) typical sorbents after 1st DRM (b) $SrCe_{0.5}Ni_{0.5}$ at different reaction stage during isothermal SLDRM process at 875 °C

Figure S2 shows the Raman analysis for $SrCe_{0.5}Ni_{0.5}$ and SrNi to evaluate type of carbon deposition. The Raman spectrum patterns in Figure S2(a) indicate only D (~1340 cm^{-1}), G (~1575 cm^{-1}) and 2D (~2682 cm^{-1}) band carbon was observed on $SrCe_{0.5}Ni_{0.5}$ and SrNi, confirming carbon deposition of graphite. As expected, the used SrCe did not contain carbon peak, indicating no carbon deposition. Figure S2(b) compares the carbon spectrum on $SrCe_{0.5}Ni_{0.5}$ at different reaction time. No detectible carbon deposition was formed in the first 2 min during the 1st DRM. It indicates that carbonates were enough for CH_4 conversion. Then, D, G and 2D band carbon were formed regardless of reaction time or cycle. Fortunately, this carbon deposition could be completely removed after carbonation and no carbon peak was observed after 30th carbonation, indicating that. It is favorable for the reactivity stability of Ni catalyst.

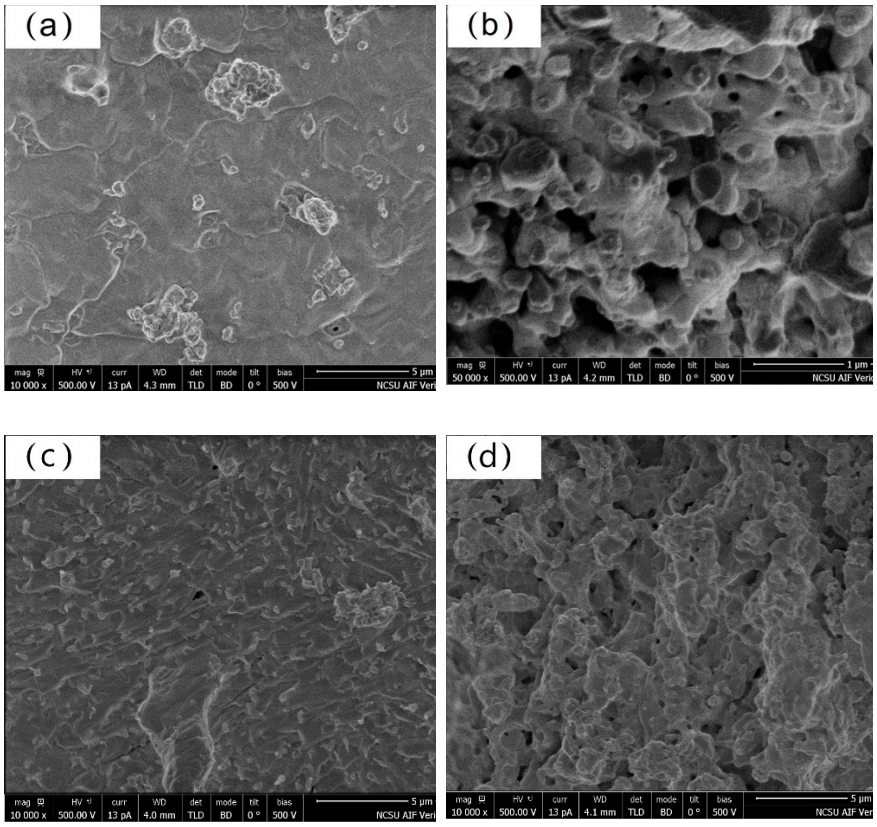

Figure S3: SEM images of $SrCe_{0.5}Ni_{0.5}$ during SLDRM process: (a) 1st carbonation, (b) 1st decarbonation (c) SEM at 30st carbonation, (d) SEM at 30st decarbonation

The microstructure is a key factor affecting the cycle performance of the selection of material. Figure S3 shows the SEM images of $SrCe_{0.5}Ni_{0.5}$ during 1st and 30th SLDRM cycle. The SEM images indicate that the smooth surface of carbonated material turned into a rough surface after decarbonation during 1st and 30th cycles. In spite of some grain agglomeration, irreversible sintering was never observed during multiple carbonation/decarbonation cycles.

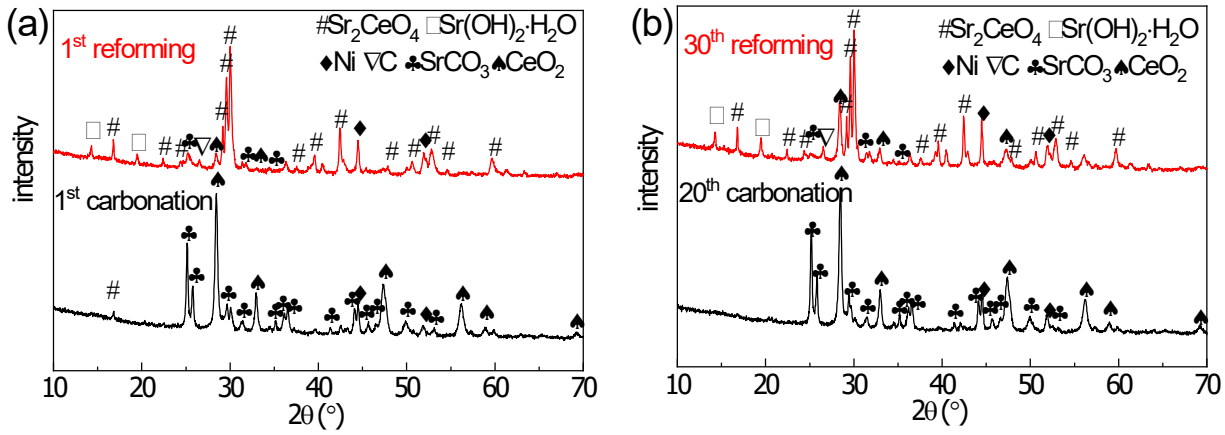

Figure S4: XRD pattern of $SrCe_{0.5}Ni_{0.5}$ during SLDRM (a) 1st cycle and (b)30th cycles.

Figure S4 shows the Xrd patterns of $SrCe_{0.5}Ni_{0.5}$ during 1st and 30th SLDRM cycle. As is shown in Figure S4(a), $SrCO_3$ and CeO_2 are two main phases in the carbonated sorbent. Then they turned into Sr_2CeO_4 as the CH_4 reforming process consuming some CO_2. Some $SrCO_3$ and CeO_2 were also observed in the reduced sample due to uncomplete decarbonation during the reforming process. In view of hygroscopic property, some $Sr(OH)_2$ instead of SrO appears in the material. The highly consistent of XRD patterns of sorbent after 30 cycle operation indicates that the material owns a perfect regeneration capacity.